Abstract

Flooding of settlements is a growing concern in Europe, also in agricultural areas. Restoration and installation of vegetated landscape elements (vLE) such as hedges, lines of trees and grass buffers, along the parcel boundaries is increasingly recognized as a way to mitigate downstream flood risk. However, there is a lack of scientific evidence to support their implementation. We used the Landlab modelling framework to gain knowledge about the importance of the presence and characteristics of vLEs for the hydrological response in a 26 hectare undulating watershed representative for the Belgian loess belt for which a multitude of vLE scenarios were developed. Our model results demonstrated that the total runoff volume, the peak discharge rate and its lag time in such small watersheds are mainly controlled by the density of the vLE objects and their upstream area. First and foremost we demonstrated a negative correlation between the discharge volume and peak discharge rate and the density of the vLE objects and their upstream area. A positive correlation was observed between the lag time and density of the vLE objects for both dry and wet soils and between the lag tag time and upstream area for dry soils. Further, we found that the impact of the value of the saturated hydraulic conductivity of the soil covered by the vLE became increasingly important with increasing soil wetness, with the hydraulic conductivity being negatively correlated with the discharge volume and peak

discharge rate. The impact of hydraulic conductivity on the lag time was limited. A negative correlation between hydraulic conductivity and lag time for intermediate wet soils was demonstrated. Our model results also showed that the roughness, expressed as the Manning n-coefficient, of the soil underneath a vLE and the spatial connectivity of the vLE objects have little impact on the hydrological response.

Revised highlights with no changes marked

Highlights

- Modelling results confirm that landscape elements contribute to lowering flood risk
- Higher initial soil wetness levels result in more and faster discharge
- Runoff is controlled by the density of landscape elements and their upstream area

Title: The impact of vegetated landscape elements on runoff in a small agricultural watershed: A modelling study

Authors names and affiliations:

Ine Rosier[A]

[A]Department of Earth and Environmental Sciences, KU Leuven, Celestijnenlaan 200E - bus 2411, B-3001 Leuven, Belgium

ine.rosier@kuleuven.be

Jan Diels[A]

[A]Department of Earth and Environmental Sciences, KU Leuven, Celestijnenlaan 200E - bus 2411, B-3001 Leuven, Belgium

jan.diels@kuleuven.be

Ben Somers[A]

[A]Department of Earth and Environmental Sciences, KU Leuven, Celestijnenlaan 200E - bus 2411, B-3001 Leuven, Belgium

ben.somers@kuleuven.be

Jos Van Orshoven[A]

[A]Department of Earth and Environmental Sciences, KU Leuven, Celestijnenlaan 200E - bus 2411, B-3001 Leuven, Belgium

jos.vanorshoven@kuleuven.be

Corresponding author: Ine Rosier (ine.rosier@kuleuven.be)

Keywords: surface runoff modeling; agricultural watershed; vegetated landscape element; natural flood management

1. Introduction

Extensive areas throughout Europe are affected by flooding of rivers or from surface runoff. This can be demonstrated by the destructive events of July 2021 in Western Europe that caused an estimated loss of up to €5.8 billion and over 200 deaths (Kreienkamp et al., 2021). In the period between 1980 and 2013, almost 1500 flood and wet mass movement events happened within the European Union, more than half of them since 2000 (EEA, 2017). In Belgium, flood events are a common occurrence in the Belgian loess belt, which covers about 34 % (10576 km²) of the Belgian territory. These flood events are often co-determined by runoff from agricultural land. Between 1991 and 2004, 79 % of the municipalities located within the Belgian loess belt were affected by floods resulting from runoff from arable land (Bielders et al., 2003; Evrard et al., 2007a). Flood hazard is likely to increase in this region as a result of the expected global-warming related changes in the frequency and magnitude of extreme precipitation events (Fowler et al., 2021; Kreienkamp et al., 2021). Climate-smart upstream land use systems, and hence climate-smart land use planning, are increasingly recognized as a way to mitigate downstream flood risk (Gabriels et al., 2022; Minang et al., 2015). Vegetated landscape elements (vLEs) such as hedges, lines of trees and grass buffers are inherent components of such climate-resilient agricultural land use systems (Burgess-Gamble et al., 2017; Ellis et al., 2021). Their typical geometrical arrangement following the edges of agricultural parcels creates networks of landscape elements. These networks alter the parcel and catchment hydrology since they create hydrological discontinuities by impeding flow paths (Mérot, 1999) or enhancing flow continuities exacerbating runoff. Hence, vLEs alter the runoff pattern and hence affect the frequency, extent, depth and duration of downstream flood events (Horn et al., 2007; Klaassen and Zwaard, 1974; Mérot, 1999; Richet et al., 2017). The attitude of landowners towards these potential natural flood protection measures is not always positive, which can partly be explained by the current lack of scientific evidence about their effectiveness (Bielders et al., 2003; Ellis et al., 2021; Wells et al., 2020). Still, there is a strong positive correlation between the probability of a landowner taking flood and erosion control measures (e.g. grass buffer strips) and the probability of having experienced runoff or erosion damage during the last decade (Bielders et al., 2003).

To design evidence-based climate-smart landscapes, quantitative information about the effect of vLEs on the runoff in a catchment is needed. vLEs and their hydrological properties have been the subject of numerous studies. These studies demonstrate that the effect of the vLE on the infiltration capacity of the soil covered by that vLE depends on the type of vLEs with grass buffers decreasing the infiltration capacity compared to some common crop types while hedges increase the infiltration capacity (Baartman et al., 2020; Holden et al., 2019). Further, it was shown that vLEs are typically associated with higher hydraulic roughness values (Baartman et al., 2020; Richet et al., 2017). This not only results in a decreased velocity of runoff but also in lower sediment transport. Previously, these studies focused mainly on the impact of vLEs on runoff at the field scale (Holden et al., 2019; Richet et al., 2017; Wallace et al., 2021). However, information on these effects at a catchment scale is at least equally important as many of the off-site consequences of flooding events have to be managed at a catchment scale. Also on the catchment scale, it becomes possible to assess the effect of the geometric characteristics of the vLEs (i.e. dimensions, position along the concentrated flow paths and connectivity) on runoff within a catchment, and to investigate how these characteristics affect the rainfall-runoff behaviours of the catchment.

With this research, we aimed to gain knowledge about the importance of the presence and characteristics of vLEs on the hydrological response of a small watershed representative of the Belgian loess belt. We used a physically-based distributed rainfall-runoff model implemented in the Landlab modelling framework (Barnhart et al., 2020; Hobley et al., 2017) to quantify the effect of various configurations and characteristics of vLEs using a design storm (Willems, 2013). Our findings are meant to aid in the conservation and promotion of vLEs in an agricultural landscape in the future. This is important as shown by the declining trend in the presence of vLEs demonstrated by the disappearance of more than half of the hedgerows between 1900 and 2002 in Flanders (Deckers et al., 2005).

The specific objectives of this research were:

1. To assess the sensitivity of the hydrological modelling framework Landlab (Barnhart et al., 2020; Hobley et al., 2017) to changes in the hydrological properties of vLEs (i.e. Manning's roughness coefficient (n) and saturated hydraulic conductivity of the underlying soil (K_s));
2. To compare the magnitude and timing of the flood peak discharge rate and the total runoff volume produced by a design storm between various configurations of vLEs;
3. To assess the impact of contrasting initial soil moisture contents on the hydrological functioning of vLEs.

2. Methodology

2.1. Rainfall-runoff model

The open-source Python-coded Landlab modelling framework (Barnhart et al., 2020; Hobley et al., 2017) was used to simulate overland flow and infiltration in a real watershed with assumed vLEs. This modelling framework has previously been used and validated to model catchment runoff (Adams et al., 2017; Reitman et al., 2019; Zhang et al., 2020). Overland flow in the Landlab modelling framework is based on the two-dimensional shallow water equations (SWE) as is the case for many physically-based hydrological models (e.g. Cea and Bladé, 2015; Defina, 2000; Warnock et al., 2014). The SWE are a simplification of the Navier-Stokes equations in the vertical direction and consist of two parts, the conservation of mass (Eq. 1) and the conservation of momentum (Eq. 2 and Eq. 3):

$$\frac{\partial h}{\partial t} + \frac{\partial q_x}{\partial x} + \frac{\partial q_y}{\partial y} = 0 \qquad (1)$$

$$\underbrace{\frac{\partial q_x}{\partial t}}_{\substack{local\\ acceleration}} + \underbrace{\frac{\partial}{\partial x}(uq_x) + \frac{\partial}{\partial y}(vq_x)}_{\substack{convective\\ acceleration}} + \underbrace{gh\frac{\partial(h+z)}{\partial x}}_{\substack{pressure+\\ bed\ gradients}} + \underbrace{\frac{gn^2\|q\|q_x}{h^{7/3}}}_{friction} = 0 \qquad (2)$$

$$\underbrace{\frac{\partial q_y}{\partial t}}_{\substack{local\\ acceleration}} + \underbrace{\frac{\partial}{\partial y}(uq_y) + \frac{\partial}{\partial x}(vq_y)}_{\substack{convective\\ acceleration}} + \underbrace{gh\frac{\partial(h+z)}{\partial y}}_{\substack{pressure+\\ bed\ gradients}} \cdot \underbrace{\frac{gn^2\|\boldsymbol{q}\|q_y}{h^{7/3}}}_{friction} = 0 \qquad (3)$$

where x [m] and y [m] are the planimetric Cartesian directions, t [s] is time, h [m] is water depth, q_x and q_y [m^2 s^{-1}] are the x and y components of the discharge per unit width vector $\boldsymbol{q}$, (u, v) [m s^{-1}] are the velocities at x, y-direction, z [m] is the bed elevation, g [m s^{-2}] is the gravity acceleration, and n [s $m^{-1/3}$] is the Manning's n. Since full Shallow Water models are computationally expensive, some studies suggest approximating or omitting specific terms in the SWE (e.g. Bates et al., 2010; Singh, 1997). We used LISFLOOD-FP, a simplified approximation of the SWE that omits the convective acceleration term in Eq. 2 and Eq. 3 (Bates et al., 2010; Bates and De Roo, 2000; de Almeida et al., 2012; de Almeida and Bates, 2013). The original python code from the Landlab library modelling framework was adapted to allow defining a unique Manning's n for each cell in the gridded watershed. This roughness coefficient was used to drive overland flow. The flow direction is determined by defining for each cell the steepest path in the four cardinal directions. The outlet was selected to be the only location in the watershed where water can exit the watershed. Therefore, all other boundary cells were set as 'no flux' cells.

For each time step, water losses due to infiltration were calculated after flow was routed by using the Green-Ampt Mein-Larson infiltration model (GAML) (Mein and Larson, 1971). GAML describes the infiltration rate as:

$$f = K_e\left(1 + \frac{\psi\Delta\theta}{F}\right) \qquad (4)$$

where f [m s^{-1}] is the potential infiltration rate, F [m] is the cumulative infiltration, ψ [m] is the capillary pressure head at the wetting front, $\Delta\vartheta$ [m^3 m^{-3}] is the difference between saturated and initial volumetric moisture content, and K_e [m s^{-1}] is the effective hydraulic conductivity. K_e is a lumped parameter that adjusts K_s to account for spatial variation in rainfall intensity and soil properties (e.g., soil crusting, surface microtopography and soil pore structure) (Langhans et al., 2010b; Van den Putte et al., 2013). The GAML describes a situation where runoff occurs only after some time, i.e. the ponding time. A minimum water depth on the surface of 1.0E-8 m that can not infiltrate was assumed. This was done to avoid numerical instability of the solutions of the overland flow modelling resulting from the calculation of negative water depths, as suggested by Costabile et al. (2012).

2.2. Model construction

2.2.1. Study area

A 26 ha agricultural watershed situated in the Belgian loess belt was selected (50.72° N, 5.12°E). This area has been repeatedly affected by floods as happens frequently in undulating agricultural areas on loamy soils in Flanders (Bielders et al., 2003; Evrard et al., 2007b). The elevation in the watershed was characterized by a 2 m resolution digital elevation model (DEM). Altitudes range between 106 m and 120 m above sea level. The majority of the land cover (94 %) in the study area is agricultural land (i.e. arable land and agricultural grassland) (ALV, 2021).

[Figure 1]

2.2.2. Vegetation cover

Existing field boundary patterns were used to generate different configurations of vLEs. The first three patterns (Figure 2, a-c) occur elsewhere in Belgium and were chosen to be representative of a typical agricultural field pattern (FP) in the region. These three patterns were selected by assessing the parcel configuration around a selection of 1000 randomly chosen agricultural fields in the region and selecting a field pattern with a small, medium and large average plot size. FP1 (Figure 2, a) is characterized by smaller plots with an average field size of 1.42 ha. FP2 (Figure 2, b) is characterized by medium-sized fields with an average size of 1.89 ha. FP3 (Figure 2, c) is characterized by larger fields with an average field size of 2.33 ha. The fourth pattern (FP4, Figure 2, d) was generated to have field boundaries perpendicular and parallel to the flow directions in the watershed.

[Figure 2]

In total, 42 configurations of vLEs were created based on the field boundaries of FP1, FP2, FP3 and FP4. These configurations differ in the density of vLEs, connectivity, and upslope area. Three different values of vLE density were used: 87 m ha^{-1}, 40 m ha^{-1} and 10 m ha^{-1}. The highest vLE density represents the mean density of vLEs in Flanders in the year 1900, while a density of 40 m ha^{-1} represents the average situation in 2002 (Deckers et al., 2005). A watershed with a vLE density of 10 m ha^{-1} represents a situation in which the density of vLEs in the landscape is further reduced, e.g. due to further intensification and heavy machinery use. For FP1, FP2 and FP3, four configurations per density level, with a range in connectivity, were generated. To do this, 10000 random combinations of field borders were selected and the beta connectivity index (β) was calculated as:

$$\beta = \frac{e}{v} \qquad (5)$$

with e the number of vLE segments and v the number of vLE nodes. A segment was defined as a side of an agricultural field boundary with the start and end point of the segment being defined as nodes. In case a start or end node of another segment was positioned along the segment, the segment was split in two at the location of that node. The two configurations of field borders with the highest β per density level were then selected. Disconnections in these two configurations were created by rotating per vLE section of 60 m, the middle 20 m with an angle of 90 degrees. This was done to assess the impact of the connectivity of vLEs without changing the density or geographical position of the vLEs. For FP4, two configurations per density level were created, one where the vLEs were mainly positioned along the flow direction in the watershed and one where they were located perpendicular to the modelled flow direction. While in FP1, FP2 and FP3 we aimed to assess the impact of vLE connectivity on runoff, we focused on vLE configurations positioned along with or perpendicular to the main slope in FP4. The vLE configurations were rasterized by assigning the land use class 'vLE' to all pixels intersected by a vLE field border. All other pixels in the watershed were considered to be 'landscape' pixels. The average number of 'vLE' pixels in the watershed was 166, 659 and 1400 for a density level of 10 m ha^{-1}, 40 m ha^{-1} and 87 m ha^{-1} respectively. This corresponds to 0.29 %, 1.14 % and 2.34 % of the total number of pixels in the watershed. For all 42 vLE configurations, the β-index (Eq. 5) and the upslope area per meter vLE were calculated. The average upslope area per meter vLE was calculated by assessing for each vLE pixel the size of the area that directly contributes water to that pixel. The sum of that area for all vLE pixels was then divided by the total length of the vLE objects in the watershed to obtain the average upslope area per meter ‘vLE’. This gives an estimation of the runoff going through the vLEs in the watershed, with larger values indicating a larger proportion of the runoff that flows through the vLE.

GAML parameters, Manning’s n and other soil parameters were selected based on values found in literature and are summarized in Table 1. We assumed that our watershed had a uniform loamy soil. The K_s, initial volumetric moisture content (ϑ_i) and capillary pressure head at wetting front were based on values derived by Van den Putte et al. (2013) from a dataset consisting of 350 rainfall experiments carried out on 21 arable fields in the Belgian loess belt. The K_s was equal to 19.2 mm hr^{-1}, which was the average effective hydraulic conductivity derived for rainfall experiments carried out in the summer period. The ϑ_i was set to a value between 0.02 cm^3 cm^{-3} and 0.29 cm^3 cm^{-3}, which are the minimum and maximum ϑ_i values measured for experiments carried out in the summer period. Further, a ϑ_i of 0.155 cm^3 cm^{-3} was used as a medium value of ϑ_i. The capillary pressure head at wetting front used in our model equals 172.7 mm, which was the average value derived for rainfall experiments carried out in the summer period. The Manning’s n was set to 0.08 s m$^{-1/3}$. This value was based on the value measured by Takken et al. (1999) for land with the maize crop. Maize was selected as the only land cover type. Maize is the crop type with the largest spatial extent in Flanders (ALV, 2021).

The vLEs were accounted for in the hydrological model by assigning adjusted values of K_s and of Manning’s n to vLE pixels. Three different values for K_s for the soil under the vLEs were selected. The first value was equal to 102.4 mm hr^{-1} which is representative of loamy soils under hedges (Holden et al., 2019). The second value was equal to 20 mm hr^{-1} which is representative of loamy soils under grass buffers (Baartman et al., 2020; Evrard et al., 2009). As a third value, an intermediate value was chosen, i.e. 51.2 mm hr^{-1}. Further, also three values of the Manning's n linked with vLEs were selected. We used 0.43 s m$^{-1/3}$ and 0.55 s m$^{-1/3}$, which are the minimum and maximum values of Manning's n for hedgerows calculated by Richet et al. (2017). Further, we also used a Manning's n of 0.30 s m$^{-1/3}$ which is the roughness coefficient associated with grass buffers (Baartman et al., 2020).

2.2.3. Precipitation data

This study uses a design storm, i.e. a hypothetical rainfall event associated with a specific duration and return period, as precipitation input in the model. Such design storms are often used for flood risk assessments (Jiang et al., 2019). The 2-hour spatially uniform design storm with a 50-year return period used in this study was calculated based on the intensity-duration-frequency (IDF) relationship derived from the Uccle 10 min rainfall time series (Demarée, 2003) for the period 1898-2007 (Willems, 2013). The calculation was done by using a frequency-based method that constructs the hyetograph from the entire IDF curve (Krvavica and Rubinić, 2020). The IDF relationship was adjusted to account for multidecadal climate oscillations (Willems, 2013). The peak intensity of the rainfall event was equal to 127.87 mm hr^{-1} while the total rainfall volume over the catchment in the considered 2-hour period was around 11000 m^3.

2.3. Model application

The rainfall-runoff model described in section 2.1 was applied for 378 vLE scenarios using Python (Version: 3.9.7). These scenarios were derived by combining varying landscape patterns, different levels of vLE density, connectivity, and values of K_s and Manning's n associated with the vLE objects (Appendix A). The 378 scenarios were run for ϑ_i equal to 0.02 m^3 m^{-3} 0.155 m^3 m^{-3} and 0.29 m^3 m^{-3}, hereafter referred to dry, intermediate wet, and wet soils. While the 50-year return period design storm had a length of 2 hours, the total model run time was set for an additional 2 hours after rainfall ceased to allow all runoff water to either reach the outlet of the watershed or infiltrate. After each model run, the total discharge volume (in m^3), the peak discharge rate at the outlet (in m^3 per second) and the lag time between the rainfall and discharge peaks (in seconds) were derived from the discharge time series.

2.4. vLE feature impact on runoff

The impact of the vLE features on the total discharge volume, the peak discharge rate and the lag time was assessed by comparing the differences in the output variables between different values of the vLE features in a multidimensional analysis on the one hand and in a one-dimensional analysis on the other hand. All statistical analyses were done using R software (Version: 4.1.2).

2.4.1. Multidimensional analysis

To take into account feature interactions and rank the importance of the impact of each considered vLE feature (density, connectivity, upslope area, Manning's n and K_s) on the output variables, 9 random forest analyses were conducted, one for each combination of output variable (3) and soil wetness level (3) using the "randomForest" package (Version: 4.7-1). A randomly selected bootstrapped sample of 70 % of the 378 scenarios was used as a training set to fit 500 classification trees. The remaining 30 % of the observations were used as a testing set to evaluate the predictive performance of the models. The relative importance of the features within the model was determined to show the impact of each input feature on the total discharge volume, the peak discharge rate and the lag time. This was done by constructing the global variable importance curves using the package "vivo" (Version: 0.2.1) and "DALEX" (Version: 2.4.1) and comparing the variable importance of each feature with the maximal variable importance in the model. Regression trees have previously proven to be successful to assess the relative impact of features (e.g., Poncelet et al., 2017).

2.4.2. One-dimensional analysis

For each unique combination of density, Manning's n and K_s, 14 vLE configurations were created (Appendix A). For these 14 configurations, the upslope area and connectivity were derived. For each of the vLE features (density, Manning's n and K_s, connectivity, upslope area), a Kruskal-Wallis nonparametric test (Kruskal and Wallis, 1952) was used to evaluate whether at least one level of these features performed significantly different from the others using the package “stats” (Version: 4.2.1). The impact of a feature on an output variable was considered significant if the P-value returned by the test was lower than 0.05. If the impact of the feature was considered significant, a subsequent post-hoc Dunn’s test with a Bonferroni correction was performed using the package “dunn.test” (Version: 1.3.5) to determine which levels of the features differ from each other. These differences were considered significant if the P-value returned by the test was lower than 0.05.

3. Results

Runoff simulations for the 378 scenarios at three different wetness levels resulted in 1134 hydrographs from which the discharge volume, peak discharge rate and lag time were derived. Initial soil moisture content was shown to have a large impact on the discharge volume, peak discharge rate and lag time. The average modelled discharge volume for all 378 scenarios was 3.08 m^3, 17.01 m^3 and 110.66 m^3 for dry, intermediate wet, and wet soil respectively. The average modelled peak discharge rate was 0.01 $m^3 s^{-1}$, 0.02 $m^3 s^{-1}$ and 0.08 $m^3 s^{-1}$ respectively, and the average modelled lag time was 360.32 s, 593.62 s and 593.17 s respectively. For dry soils, discharge in the watershed is dominated by runoff from a relatively small area close to the outlet as a large portion of the runoff from areas further away from the outlet can infiltrate and will not reach the outlet. This results in a discharge peak that closely follows the peak in rainfall. For wet soils, however, a smaller proportion of the precipitation will infiltrate and more runoff will reach the outlet of the watershed. Runoff from areas further away from the outlet has longer travel times and therefore the peak in discharge will arrive later in time for wet soils. An illustration of the hydrograph of four distinct scenarios for wet soils with the associated hyetograph is given in Figure 3. The bimodal shape of the hydrographs is the result of different flow paths arriving at the outlet. The flow path conveying water from an area close to the outlet of the watershed results in a peak in discharge close to the peak in the rainfall. The flow path conveying water from an area at a larger distance from the outlet results in a peak of discharge later in time. The vLE characteristics of the four scenarios and their corresponding discharge volume, peak discharge rate and lag time values are given in Table 2.

[Figure 3]

3.1. Multidimensional analysis

We used random forest regression models to take into account feature interactions and rank the importance of the impact of each considered feature on the output variables. The regression models explained 98 % of the variation of the output variable 'discharge volume' for all three wetness levels, between 96 % and 98 % of the variation of the output variable 'peak discharge rate' and between 33 % and 84 % of the variation of the output variable 'lag time' (Table 3). The relatively low R^2 value for wet soils suggests there could be other variables influencing the lag time after a storm than the variables here considered. Our analysis revealed that the vLE features with the highest impact on the output variables differ per output variable and soil wetness level (Figure 4). The vLE density in the watershed and the upslope area of the vLE objects were the two most important features in 7 out of 9 random forest models. For explaining the total discharge volume and peak discharge rate in wet soil conditions, the two most important variables were the K_s value associated with the vLE object and the upslope area of the vLE objects. The impact of connectivity of the vLE network on the total discharge volume and peak discharge rate was limited, but an increase of relative impact could be observed with increasing values of ϑ_i. A higher impact of connectivity of the vLE network on the lag time was observed, where the impact of the connectivity on the lag time decreased with increasing values of ϑ_i. Increasing soil wetness resulted in a higher relative impact of the K_s value associated with the vLE object on the total discharge volume and the peak discharge rate. This was not the case when the lag time was evaluated whereby the impact of the K_s value was limited for wet and dry soils. The Manning's n associated with the vLE objects had little impact on all three output variables.

[Figure 4]

3.2. One-dimensional analysis

A Kruskal-Wallis test was performed to identify whether at least one level of the considered vLE feature performed significantly different from the others. This was done for the output variable discharge volume, peak discharge rate and lag time. The considered vLE features were vLE density, the connectivity of the vLE configuration expressed as *β*, the upslope area of the vLEs, the K_s associated with the soil underneath the vLEs, and the Manning's n associated with the vLEs. The results are presented in Table 4.

3.2.1. Effect of density of vLE objects

The vLE density had a generally negative impact on the total discharge volume and peak discharge rate and a positive impact on the lag time: the larger the vLE density in the watershed, the lower the total discharge volume and peak discharge rate and the larger the lag time (Figure 5). These effects could also be seen when the storm hydrographs for scenarios with different density levels were compared (Figure 3 and Table 2, scenarios 1, 2, 3). An exception to this trend was observed when the median lag times between a vLE density of 10 m ha^{-1} and of 40 m ha^{-1} for wet soils were compared. In this case, the lag time decreases with increasing vLE density. For all soil wetness levels, the Kruskal-Wallis test demonstrates that these differences were statistically significant when the discharge volume and peak discharge rate were evaluated (P-value < 0.05). These differences were more prominent with increasing levels of initial soil moisture. For the output variable 'lag time', no statistically significant differences were found between different levels of vLE density for intermediate wet soils. However, for dry and wet soils, statistically significant differences were found (P-value < 0.05) between different levels of vLE density.

[Figure 5]

3.2.2. Effect of connectivity

The connectivity of the vLE network had little impact on the total discharge volume, peak discharge rate and lag time (Figure 6). A Kruskal-Wallis test showed only a statistically significant difference between different levels of connectivity for the total discharge volume and peak discharge rate for dry soils (Table 4). Contrary to our expectations, we found that increasing values of the β-index (i.e. higher connectivity in the vLE network) result in a higher total discharge volume and higher peak discharge rates. No statistically significant differences were found between the different levels of connectivity and the lag time for dry soils, nor for any of the output variables for dry or intermediate wet soils.

[Figure 6]

3.2.3. Effect of upslope area

The upslope area had a statistically significant negative impact on the total discharge volume and peak discharge rate for dry and wet soils and a significant positive impact on the lag time for dry soils (Figure 7 & Table 4). Different levels of upslope area in wet soils were shown to also have significant differences in lag time values but no uniform trend could be distinguished. The post-hoc Dunn's test demonstrated that for the lower levels of upslope area, lag time decreased with increasing values of upslope area, while the highest level of upslope area was associated with significantly higher values of the lag time. The effects can also be observed when the storm hydrographs for scenarios with different density levels are compared (Figure 3 and Table 2, scenarios 1 & 2). While the Kruskal-Wallis test identified significant differences in the total discharge volume and peak discharge rate between different levels of upslope area in intermediate wet soils, no clear trend could be observed. Intermediate wet soils did not show any significant differences in lag time between different levels of upslope area.

[Figure 7]

3.2.4. *Effect of saturated hydraulic conductivity*

A higher K_s associated with the soil underneath the vLE objects had a generally negative impact on the total discharge volume and peak discharge rate: the larger the K_s value, the lower the total discharge volume and peak discharge rate (Figure 8). These effects could also be seen when the storm hydrographs for scenarios with different levels of K_s values are compared (Figure 3 and Table 2, scenarios 3 & 4). The differences in total discharge volume and peak discharge rate between the different K_s levels were statistically not significant for dry soils (Table 4). The K_s value associated with the vLE objects was proven to have a limited impact on the lag time. Only for intermediate wet soils, statistically significant differences could be identified for the lag time when different levels of K_s were considered, with increasing levels of K_s resulting in a modest decrease in lag time. The modelled difference between the median lag time of the lowest and highest level of K_s was only 0.04 seconds (Figure 8 & Table 4).

[Figure 8]

3.2.5. *Effect of Manning's roughness coefficient*

The Kruskal-Wallis tests revealed no statistically significant differences between the different levels of the Manning's n and the three output variables (Figure 9 & Table 4).

[Figure 9]

4. Discussion

4.1. Model construction

We used the distributed rainfall-runoff model, implemented in the Landlab modelling framework, to quantify the impact of vLEs and their geometric and hydrological characteristics on runoff in a small watershed. Obviously, reality was simplified in multiple ways in the model setup. A spatially uniform rainfall event was assumed while in reality, rainfall is heterogeneously distributed over the catchment. Interception of rainfall by vegetation was not taken into account, neglecting the interception of rainfall that lowers the amount that reaches the soil surface. These interception losses occur both at the location of the agricultural land and vLE objects. It was quantified that hedgerows for example can intercept up to 2.6 mm of a precipitation event (Herbst et al., 2006). By not taking these interception losses into account, the rainfall amount that reaches the soil surface was overestimated. We also assumed that the soil parameters (i.e., ϑ_i, capillary pressure head at wetting front, K_s and Manning's n) were spatially uniform in our watershed. These values were, if available, based on values found in literature reports about experimental studies done in the same region as our study area. For hedgerows, we did not find K_s values measured in the Belgian loam belt in the literature. Therefore we used a value measured in a loamy soil in northern England. Field studies usually show a large heterogeneity in soil wetness, both in the horizontal and vertical dimensions (Merz and Plate, 1997). This spatial heterogeneity can be attributed to a variety of factors including variations in soil characteristics, topography, and water routing processes (Merz and Plate, 1997). The presence of vLEs also has an impact on soil moisture, not only directly underneath the object but also up to 10 m beyond their peripheries (Wallace et al., 2021). The overland flow routing and therefore the infiltration was calculated based on a 2 m resolution DEM. At this spatial resolution, non-random microtopography-related variations of K_s (Langhans et al., 2010a) cannot be accounted for and the model assumes water is uniformly spread over the pixel. This results in an overestimation of the effective hydraulic conductivity that is dependent on the inundated fraction of the pixel, and therefore also in an overestimation of the fraction of the precipitation that can infiltrate. We calculated an average runoff coefficient (i.e., the total runoff volume divided by the total precipitation volume) of 0.0003 $m^3\ m^{-3}$ for $\vartheta_i = 0.02\ m^3\ m^{-3}$, 0.0015 $m^3\ m^{-3}$ for $\vartheta_i = 0.155\ m^3\ m^{-3}$ and 0.0101 $m^3\ m^{-3}$ for $\vartheta_i = 0.29\ m^3\ m^{-3}$. These values are slightly lower but in the same range as the findings of Evrard et al. (2007b) and Evrard et al. (2008) who conducted a hydrological study near our study area. The slightly lower values of the runoff coefficients we calculated could be explained by an overestimation of the K_s values used in this study. Hydraulic conductivity has been proven to be dependent on water depth and rainfall intensity due to non-random microtopography (Langhans et al., 2013). The K_s value used for the 'landscape' pixels, which covers the vast majority of the study area, was derived from rainfall experiments with an intensity of ca. 45 mm h^{-1} (Van den Putte et al., 2013). The design storm used in this study had an intensity lower than 45 mm h^{-1} for 92 % of the duration of the storm. Earlier research carried out on loam soils in Belgium has demonstrated a positive correlation between rainfall intensity and hydraulic conductivity (Langhans et al., 2010b). This implies an overestimation of the K_s value was made during the majority of the time covered by the modelled storm over our watershed and could have resulted in underestimated values of the runoff coefficient. Further, K_s has proven to be highly variable in the study region. Van den Putte et al. (2013) calculated a standard deviation of obtained hydraulic conductivity values of 13.4 mm h^{-1} for rainfall experiments carried out in the summer period. This high variability could have potentially led to an overestimation of K_s in our study area. Lastly, the observed runoff coefficients were derived for a catchment in which the average slope was 24 % higher compared to the study area used here. Catchments with higher slopes typically show higher values of the runoff coefficient (De Niel and Willems, 2019).

4.2. Impact of vLEs on runoff

The impact of the vLE density, connectivity, upslope area, K_s and Manning's n on the modelled total discharge volume, peak discharge rate and lag time was evaluated (Figure 4). A negative correlation was found between vLE density and discharge volume and peak discharge rate and a positive correlation between vLE density and lag time (Figure 5). These findings are in line with previous research based on field experiments where higher vLE densities could be associated with increased infiltration, lower discharge volumes and peak discharge rates (Mérot, 1999; Viaud et al., 2005). Due to longer travel times and increased infiltration, the storm hydrograph is smoothed out (i.e., the lag time is longer and the peak discharge rate is reduced) in catchments with higher densities of vLEs (Mérot, 1999). This is also visualized in Figure 3 (scenarios 1, 2, 3): while K_s, Manning's n and β remain completely, or nearly constant across the 3 scenarios, an increase in vLE density ρ results in a lower discharge volume and peak discharge rate and a larger lag time, regardless of changes in upslope area. Therefore, it is recommended that the number of vLEs in the agricultural landscape does not further decrease, and better even, increases.

Besides testing the impact of vLE density, we also looked at the effect of the connectivity of vLEs in the landscape by creating disconnections in the vLE objects. In reality, the connectivity of the vLE network in a landscape context is interrelated with the density of that vLE network: denser vLE networks also demonstrate a higher level of connectivity

(Burel and Baudry, 2012; Deckers et al., 2005). By keeping the density constant, we aimed at studying the effect of the connectivity independently of the vLE density. No strong impact of vLE connectivity on catchment runoff was found (Figure 4). The correlations between the level of connectivity and the discharge volume on the one hand and peak discharge rate, on the other hand, were both weakly negative and only present when the initial soil moisture content is low (Figure 6). The upslope area of the vLE objects showed to have a strong impact on the total discharge volume, the peak discharge rate and the lag time (Figure 4). In both dry and wet soils, we identified a negative relationship between the upslope area of the vLE objects and the discharge volume and peak discharge rate. This is in line with our expectations and indicates that vLE objects positioned on preferential flow paths downstream in the watershed can make a greater difference. When vLEs are associated with large values of the upslope area, a large proportion of the runoff will flow to the footprint of the vLE object. Due to the higher K_s values associated with vLE objects compared to the landscape pixels, more water can infiltrate. This is the concept behind the installation of grassed waterways where an increase of infiltration is achieved by decreasing runoff velocities through increasing the roughness and K_s (Evrard et al., 2008). The negative relationship between upslope area and peak discharge rate and the positive relationship with lag time can also be observed when the storm hydrographs were compared (Figure 3, scenarios 1 & 2): while all other vLE characteristics remain constant, an increase in the upslope area results in a decrease of the discharge volume and peak discharge rate and an increase in the lag time.

vLE objects are associated with values of K_s that are up to 30 times higher compared to the surrounding agricultural land (Holden et al., 2019), which enhances infiltration. We could observe this effect in our modelling results where higher values of K_s associated with the vLEs result in a decrease of the discharge volume (Figure 8). We found an increase of the impact of the K_s value associated with the vLE object on discharge volume and peak discharge rate with increasing levels of soil wetness. This is contradictory to the findings of Hu et al. (2015) who concluded that the impact of K_s variability on runoff increased for lower ϑ_i values. Besides their higher K_s values, vLE objects are also characterized by higher values of Manning's n compared to surrounding agricultural land (Baartman et al., 2020; Richet et al., 2017). This increase in roughness is expected to reduce the velocity of the overland flow and thereby promoting infiltration and reducing the total runoff volume (Ferguson and Fenner, 2020). We did however not see this effect in our modelling results.

We applied the rainfall-runoff model to a relatively small watershed (26 ha) to quantify the impact of vLEs and their characteristics on runoff by using a design storm. In larger catchments, the river network configuration determines which areas of the catchment have the largest impact on the discharge peak while in small catchments this peak is dominated by run-off from hillslopes in response to the storm (Dadson et al., 2017; Mérot, 1999). Therefore, it cannot be assumed that the effect of small-scale interventions can simply be extrapolated to estimate the combined effect at a larger scale (Dadson et al., 2017).

5. Conclusions

Using a distributed rainfall-runoff model, we demonstrated that total discharge volume, peak discharge rate and lag time to peak discharge are impacted more by the density of the vLE objects (positioned along the parcel boundaries) in the watershed and their upslope area in comparison to the vLE-connectivity, the saturated hydraulic conductivity of the soil underneath the vLE and the Manning's n coefficient associated with the vLE. The initial soil wetness level does not alter this relationship fundamentally.

Both for upslope area and vLE density, a negative correlation with the total discharge volume and peak discharge rate and a positive correlation with the lag time was demonstrated. The relationship is not linear though: e.g., a factor 8.7 increase in linear density leads to a reduction of some 20 % in discharge volume. The modelled impact of the K_s value associated with the soil underneath the vLE objects on the discharge volume and peak discharge rate was rather weak but increased with increasing wetness. K_s was shown to be negatively correlated with the discharge volume and peak discharge rate. Connectivity and the Manning's n value associated with the vLE objects had a limited impact on the modelled discharge volume, peak discharge rate and lag time. The connectivity of the vLE network had little impact on the total discharge volume, peak discharge rate and lag time

We conclude that the more abundant the vLE along the agricultural parcel boundaries, the more rainfall is retained in the watershed. Hence, our modelling study confirms that vLEs contribute to a non-negligible extent to lowering the downstream flood risk and increasing the time lag to peak discharge, providing more opportunities for implementing punctual security measures.

Funding: This research was funded by Fonds Wetenschappelijk Onderzoek (FWO), grant number 1SB6821N

6. References

Adams, J.M., Gasparini, N.M., Hobley, D.E.J., Tucker, G.E., Hutton, E.W.H., Nudurupati, S.S., Istanbulluoglu, E., 2017. The Landlab v1.0 OverlandFlow component: a Python tool for computing shallow-water flow across watersheds. Geosci. Model Dev. 10, 1645–1663. https://doi.org/10.5194/gmd-10-1645-2017

ALV, 2021. Dataserie Landbouwgebruikspercelen 2021. [WWW Document]. URL https://www.geopunt.be/catalogus/datasetfolder/7cc9babc-e021-46bc-abb6-1b74d44b14ea (accessed 4.14.22).

Baartman, J.E.M., Nunes, J.P., Masselink, R., Darboux, F., Bielders, C., Degré, A., Cantreul, V., Cerdan, O., Grangeon, T., Fiener, P., Wilken, F., Schindewolf, M., Wainwright, J., 2020. What do models tell us about water and sediment connectivity? Geomorphology 367, 107300. https://doi.org/10.1016/j.geomorph.2020.107300

Barnhart, K.R., Hutton, E.W.H., Tucker, G.E., Gasparini, N.M., Istanbulluoglu, E., Hobley, D.E.J., Lyons, N.J., Mouchene, M., Nudurupati, S.S., Adams, J.M., 2020. Short communication: Landlab v2. 0: a software package for Earth surface dynamics. Earth Surf. Dynam. 8, 379–397. https://doi.org/doi.org/10.5194/esurf-8-379-2020

Bates, P.D., De Roo, A.P.J., 2000. A simple raster-based model for flood inundation simulation. J. Hydrol. 236, 54–77. https://doi.org/10.1016/S0022-1694(00)00278-X

Bates, P.D., Horritt, M.S., Fewtrell, T.J., 2010. A simple inertial formulation of the shallow water equations for efficient two-dimensional flood inundation modelling. J. Hydrol. 387, 33–45. https://doi.org/10.1016/j.jhydrol.2010.03.027

Bielders, C.L., Ramelot, C., Persoons, E., 2003. Farmer perception of runoff and erosion and extent of flooding in the silt-loam belt of the Belgian Walloon Region. Environ. Sci. Policy 6, 85–93. https://doi.org/10.1016/S1462-9011(02)00117-X

Burel, F., Baudry, J., 2012. Hedgerow connectivity. Hedgelink. Université, Staffordshire, GBR., Staffordshire, United Kingdom.

Burgess-Gamble, L., Ngai, R., Wilkinson, M., Nisbet, T., Pontee, N., Harvey, R., Kipling, K., Addy, S., Rose, S., Maslen, S., 2017.

Working with natural processes–evidence directory (No. SC150005). Environment Agency, Bristol, UK.

Cea, L., Bladé, E., 2015. A simple and efficient unstructured finite volume scheme for solving the shallow water equations in overland flow applications. Water Resour. Res. 51, 5464–5486. https://doi.org/10.1002/2014WR016547

Costabile, P., Costanzo, C., Macchione, F., Mercogliano, P., 2012. Two-dimensional model for overland flow simulations: A case study. Eur. Water 38, 13–23.

Dadson, S.J., Hall, J.W., Murgatroyd, A., Acreman, M., Bates, P., Beven, K., Heathwaite, L., Holden, J., Holman, I.P., Lane, S.N., O'Connell, E., Penning-Rowsell, E., Reynard, N., Sear, D., Thorne, C., Wilby, R., 2017. A restatement of the natural science evidence concerning catchment-based 'natural' flood management in the UK. Proceedings of the Royal Society A: Mathematical, Physical and Engineering Sciences 473, 20160706. https://doi.org/10.1098/rspa.2016.0706

de Almeida, G.A.M., Bates, P., 2013. Applicability of the local inertial approximation of the shallow water equations to flood modeling. Water Resour. Res. 49, 4833–4844. https://doi.org/10.1002/wrcr.20366

de Almeida, G.A.M., Bates, P., Freer, J.E., Souvignet, M., 2012. Improving the stability of a simple formulation of the shallow water equations for 2-D flood modeling. Water Resour. Res. 48, 14. https://doi.org/10.1029/2011WR011570

De Niel, J., Willems, P., 2019. Climate or land cover variations: what is driving observed changes in river peak flows? A data-based attribution study. Hydrol. Earth Syst. Sci. 23, 871–882. https://doi.org/10.5194/hess-23-871-2019

Deckers, B., Kerselaers, E., Gulinck, H., Muys, B., Hermy, M., 2005. Long-term spatio-temporal dynamics of a hedgerow network landscape in Flanders, Belgium. Environ. Conserv. 32, 20–29. https://doi.org/doi:10.1017/S0376892905001840

Defina, A., 2000. Two-dimensional shallow flow equations for partially dry areas. Water Resour. Res. 36, 3251–3264. https://doi.org/10.1029/2000WR900167

Demarée, G.R., 2003. The centennial recording Raingauge of the Uccle Plateau its History, its Data and its Applications. Prog. Phys. Geogr. 89, 95–102. https://doi.org/10.1051/lhb/2003082

EEA, 2017. Climate change, impacts and vulnerability in Europe 2016: An indicator-based report (No. 1). European Environment Agency, Copenhagen, Denmark.

Ellis, N., Anderson, K., Brazier, R., 2021. Mainstreaming natural flood management: A proposed research framework derived from a critical evaluation of current knowledge. Progress in Physical Geography: Earth and Environment 45, 819–841. https://doi.org/10.1177/0309133321997299

Evrard, O., Bielders, C.L., Vandaele, K., van Wesemael, B., 2007a. Spatial and temporal variation of muddy floods in central Belgium, off-site impacts and potential control measures. CATENA 70, 443–454. https://doi.org/10.1016/j.catena.2006.11.011

Evrard, O., Cerdan, O., van Wesemael, B., Chauvet, M., Le Bissonnais, Y., Raclot, D., Vandaele, K., Andrieux, P., Bielders, C., 2009. Reliability of an expert-based runoff and erosion model: Application of STREAM to different environments. CATENA 78, 129–141. https://doi.org/10.1016/j.catena.2009.03.009

Evrard, O., Persoons, E., Vandaele, K., Van Wesemael, B., 2007b. Effectiveness of erosion mitigation measures to prevent muddy floods: a case study in the Belgian loam belt. Agric. Ecosyst. Environ. 118, 149–158.

Evrard, O., Vandaele, K., van Wesemael, B., Bielders, C.L., 2008. A grassed waterway and earthen dams to control muddy floods from a cultivated catchment of the Belgian loess belt. Geomorphology 100, 419–428. https://doi.org/10.1016/j.geomorph.2008.01.010

Ferguson, C., Fenner, R., 2020. The impact of Natural Flood Management on the performance of surface drainage systems: A case study in the Calder Valley. J. Hydrol. 590, 125354. https://doi.org/10.1016/j.jhydrol.2020.125354

Fowler, H.J., Lenderink, G., Prein, A.F., Westra, S., Allan, R.P., Ban, N., Barbero, R., Berg, P., Blenkinsop, S., Do, H.X., Guerreiro, S., Haerter, J.O., Kendon, E.J., Lewis, E., Schaer, C., Sharma, A., Villarini, G., Wasko, C., Zhang, X., 2021. Anthropogenic intensification of short-duration rainfall extremes. Nat. Rev. Earth Environ. 2, 107–122. https://doi.org/10.1038/s43017-020-00128-6

Gabriels, K., Willems, P., Van Orshoven, J., 2022. An iterative runoff propagation approach to identify priority locations for land cover change minimizing downstream river flood hazard. Landsc. Urban Plan. 218, 104262. https://doi.org/10.1016/j.landurbplan.2021.104262

Herbst, M., Roberts, J.M., Rosier, P.T.W., Gowing, D.J., 2006. Measuring and modelling the rainfall interception loss by hedgerows in southern England. Agric. For. Meteorol 141, 244–256. https://doi.org/10.1016/j.agrformet.2006.10.012

Hobley, D.E.J., Adams, J.M., Nudurupati, S.S., Hutton, E.W.H., Gasparini, N.M., Istanbulluoglu, E., Tucker, G.E., 2017. Creative computing with Landlab: an open-source toolkit for building, coupling, and exploring two-dimensional numerical models of Earth-surface dynamics. Earth Surf. Dynam. 5, 21–46. https://doi.org/10.5194/esurf-5-21-2017

Holden, J., Grayson, R.P., Berdeni, D., Bird, S., Chapman, P.J., Edmondson, J.L., Firbank, L.G., Helgason, T., Hodson, M.E., Hunt, S.F.P., Jones, D.T., Lappage, M.G., Marshall-Harries, E., Nelson, M., Prendergast-Miller, M., Shaw, H., Wade, R.N., Leake, J.R.,

2019. The role of hedgerows in soil functioning within agricultural landscapes. Agric. Ecosyst. Environ. 273, 1–12. https://doi.org/10.1016/j.agee.2018.11.027

Horn, R., Vossbrink, J., Peth, S., Becker, S., 2007. Impact of modern forest vehicles on soil physical properties. For. Ecol. Manage. 248, 56–63. https://doi.org/10.1016/j.foreco.2007.02.037

Hu, W., She, D., Shao, M., Chun, K.P., Si, B., 2015. Effects of initial soil water content and saturated hydraulic conductivity variability on small watershed runoff simulation using LISEM. Hydrol. Sci. J 60, 1137–1154. https://doi.org/10.1080/02626667.2014.903332

Jiang, X., Yang, L., Tatano, H., 2019. Assessing Spatial Flood Risk from Multiple Flood Sources in a Small River Basin: A Method Based on Multivariate Design Rainfall. Water 11, 1031. https://doi.org/10.3390/w11051031

Klaassen, G.J., Zwaard, J.J.V.D., 1974. Roughness Coefficients Of Vegetated Flood Plains. J. Hydraul. Res. 12, 43–63. https://doi.org/10.1080/00221687409499757

Kreienkamp, F., Philip, S.Y., Tradowsky, J.S., Kew, S.F., Lorenz, P., Arrighi, J., Belleflamme, A., Bettmann, T., Caluwaerts, S., Chan, S.C., Ciavarella, A., De Cruz, L., de Vries, H., Demuth, N., Ferrone, A., Fischer, rich M., Fowler, H.J., Goergen, K., Heinrich, D., Henrichs, Y., Lenderink, G., Kaspar, F., Nilson, E., Otto, F.E.L., Ragone, F., Seneviratne, S.I., Singh, R.K., Skålevåg, A., Termonia, P., Thalheimer, L., van Aalst, M., Van den Bergh, J., Van de Vyver, H., Vannitsem, S., van Oldenborgh, G.J., Van Schaeybroeck, B., Vautard, R., Vonk, D., Wanders, N., 2021. Rapid attribution of heavy rainfall events leading to the severe flooding in Western Europe during July 2021. World weather attribution.

Kruskal, W.H., Wallis, W.A., 1952. Use of Ranks in One-Criterion Variance Analysis. J. Am. Stat. Assoc. 47, 583–621. https://doi.org/10.1080/01621459.1952.10483441

Krvavica, N., Rubinić, J., 2020. Evaluation of Design Storms and Critical Rainfall Durations for Flood Prediction in Partially Urbanized Catchments. Water 12, 2044. https://doi.org/10.3390/w12072044

Langhans, C., Govers, G., Diels, J., 2013. Development and parameterization of an infiltration model accounting for water depth and rainfall intensity. Hydrol. Processes 27, 3777–3790. https://doi.org/10.1002/hyp.9491

Langhans, C., Govers, G., Diels, J., 2010a. Effective Hydraulic Conductivity of Partially Inundated Surfaces: Loamy Agricultural Soils, in: AGU Fall Meeting Abstracts. Presented at the AGU Fall Meeting, San Francisco, California, pp. H11C-0816.

Langhans, C., Govers, G., Diels, J., Clymans, W., Van den Putte, A., 2010b. Dependence of effective hydraulic conductivity on rainfall intensity: loamy agricultural soils. Hydrol. Processes 24, 2257–2268. https://doi.org/10.1002/hyp.7800

Mein, R.G., Larson, C.L., 1971. Modeling the Infiltration Component of the Rainfall-Runoff Process (No. 43). Water Resources Research Center (WRRC), University of Minnesota, Minneapolis, Minnesota, USA.

Mérot, P., 1999. The influence of hedgerow systems on the hydrology of agricultural catchments in a temperate climate. Agronomie 19, 655–669.

Merz, B., Plate, E.J., 1997. An analysis of the effects of spatial variability of soil and soil moisture on runoff. Water Resour. Res. 33, 2909–2922. https://doi.org/10.1029/97WR02204

Minang, P.A., van Noordwijk, M., Freeman, O.E., Mbow, C., de Leeuw, J., Catacutan, D., 2015. Climate-Smart Landscapes: Multifunctionality in Practice. World Agroforestry Center (ICRAF), Nairobi, Kenya.

Poncelet, C., Merz, R., Merz, B., Parajka, J., Oudin, L., Andréassian, V., Perrin, C., 2017. Process-based interpretation of conceptual hydrological model performance using a multinational catchment set. Water Resour. Res. 53, 7247–7268. https://doi.org/10.1002/2016WR019991

Reitman, N.G., Mueller, K.J., Tucker, G.E., Gold, R.D., Briggs, R.W., Barnhart, K.R., 2019. Offset Channels May Not Accurately Record Strike-Slip Fault Displacement: Evidence From Landscape Evolution Models. J. Geophys. Res. Solid Earth 124, 13427–13451. https://doi.org/10.1029/2019JB018596

Richet, J.-B., Ouvry, J.-F., Saunier, M., 2017. The role of vegetative barriers such as fascines and dense shrub hedges in catchment management to reduce runoff and erosion effects: Experimental evidence of efficiency, and conditions of use. Ecol. Eng. 103, 455–469. https://doi.org/10.1016/j.ecoleng.2016.08.008

Singh, V.P., 1997. Kinematic Wave Modeling in Water Resources: Environmental Hydrology. John Wiley & Sons.

Takken, I., Beuselinck, L., Nachtergaele, J., Govers, G., Poesen, J., Degraer, G., 1999. Spatial evaluation of a physically-based distributed erosion model (LISEM). CATENA 37, 431–447. https://doi.org/10.1016/S0341-8162(99)00031-4

Van den Putte, A., Govers, G., Leys, A., Langhans, C., Clymans, W., Diels, J., 2013. Estimating the parameters of the Green–Ampt infiltration equation from rainfall simulation data: Why simpler is better. J. Hydrol. 476, 332–344. https://doi.org/10.1016/j.jhydrol.2012.10.051

Viaud, V., Durand, P., Mérot, P., Sauboua, E., Saadi, Z., 2005. Modeling the impact of the spatial structure of a hedge network on the hydrology of a small catchment in a temperate climate. Agric. Water Manag. 74, 135–163. https://doi.org/10.1016/j.agwat.2004.11.010

Wallace, E.E., McShane, G., Tych, W., Kretzschmar, A., McCann, T., Chappell, N.A., 2021. The effect of hedgerow wild-margins on topsoil hydraulic properties, and overland-flow incidence, magnitude and water-quality. Hydrol. Processes 35, e14098. https://doi.org/10.1002/hyp.14098

Warnock, A., Kim, J., Ivanov, V., Katopodes, N.D., 2014. Self-Adaptive Kinematic-Dynamic Model for Overland Flow. J. Hydraul. Eng. 140, 169–181. https://doi.org/10.1061/(ASCE)HY.1943-7900.0000815

Wells, J., Labadz, J.C., Smith, A., Islam, Md.M., 2020. Barriers to the uptake and implementation of natural flood management: A social-ecological analysis. J. Flood Risk Manag. 13, e12561. https://doi.org/10.1111/jfr3.12561

Willems, P., 2013. Adjustment of extreme rainfall statistics accounting for multidecadal climate oscillations. J. Hydrol. 490, 126–133. https://doi.org/10.1016/j.jhydrol.2013.03.034

Zhang, R., Zen, R., Xing, J., Arsa, D.M.S., Saha, A., Bressan, S., 2020. Hydrological Process Surrogate Modelling and Simulation with Neural Networks, in: Lauw, H.W., Wong, R.C.-W., Ntoulas, A., Lim, E.-P., Ng, S.-K., Pan, S.J. (Eds.), Advances in Knowledge Discovery and Data Mining. Presented at the PAKDD 2020, Springer, Cham, pp. 449–461. https://doi.org/doi.org/10.1007/978-3-030-47436-2_34

Appendix

Overview of the 378 scenarios combining varying landscape patterns, different levels of vLE density, connectivity, and values of K_s and Manning's n associated with the vLE objects. For each configuration, 9 unique combinations of K_s and Manning's n were modelled (indicated by the dotted lines).

[Figure A.1]

Table 1. Hydro-physical parameters used in the distributed rainfall-runoff model.

Parameter	Unit	Value(s)
ϑ_i	$cm^3\ cm^{-3}$	0.02 – 0.155 – 0.29
Capillary pressure head at wetting front	mm	172.7
Landscape pixels		
K_s	$mm\ hr^{-1}$	19.2
Manning's n	$s\ m^{-1/3}$	0.08
vLE pixels		
K_s	$mm\ hr^{-1}$	20 – 51.2 – 102.4
Manning's n	$s\ m^{-1/3}$	0.30 – 0.43 – 0.55

Table 2. Description of four distinct model scenarios and their associated output for ϑ_i = 0.29 $m^3\ m^{-3}$.

	vLE characteristics				**Output variables**			
scenario	**density ($m\ ha^{-1}$)**	**K_s ($mm\ h^{-1}$)**	**Manning's n ($s\ m^{-1/3}$)**	**β (-)**	**Upslope area ($ha\ m^{-1}$ vLE)**	**Discharge volume (m^3)**	**Peak discharge rate ($m^3\ s^{-1}$)**	**Lag time (s)**
1	10	102.4	0.43	0.55	8.0	94	0.067	623
2	10	102.4	0.43	0.55	1.3	126	0.086	590
3	87	102.4	0.43	0.58	4.0	66	0.047	706
4	87	20	0.43	0.58	4.0	109	0.071	693

Table 3. Accuracy of the random forest regression models applied on the testing set of vLE-scenarios predicting discharge volume, peak discharge rate and lag time for ϑ_i = 0.02 $m^3\ m^{-3}$, ϑ_i = 0.155 $m^3\ m^{-3}$ and ϑ_i = 0.29 $m^3\ m^{-3}$.

	Discharge volume (m^3)		**Peak discharge rate ($m^3\ s^{-1}$)**		**Lag time (s)**	
	RMSE	**R^2**	**RMSE**	**R^2**	**RMSE**	**R^2**
ϑ_i = 0.02 m^3/m^{-3}	8.11E-02	0.98	2.79E-04	0.97	9.55E+00	0.84
ϑ_i = 0.155 m^3/m^{-3}	5.36E-01	0.98	6.70E-04	0.96	2.91E+01	0.84
ϑ_i = 0.29 m^3/m^{-3}	2.24E+00	0.98	1.35E-03	0.98	5.45E+01	0.33

Table 4. Summary of the Kruskal-Wallis test results for different levels of initial soil moisture content (ϑ_i).

Feature	Output variable	χ^2 (P-value)		
		ϑ_i = 0.02 $m^3\ m^{-3}$	ϑ_i = 0.155 $m^3\ m^{-3}$	ϑ_i = 0.29 $m^3\ m^{-3}$
vLE density	Discharge volume	65.179 (7.024E-15)**	140.580 (< 2.2E-16)**	171.530 (< 2.2E-16)**
	Peak discharge rate	45.411 (1.378E-10)**	147.760 (< 2.2E-16)**	136.070 (< 2.2E-16)**
	Lag time	38.516 (4.330E-09)**	5.551 (0.062)	32.745 (7.754E-08)**
Connectivity	Discharge volume	4.097 (0.043)*	1.324 (0.250)	2.231 (0.135)
	Peak discharge rate	5.751 (0.016)*	0.418 (0.518)	3.359 (0.067)
	Lag time	0.224 (0.636)	1.546 (0.214)	1.514 (0.219)
Upslope area	Discharge volume	71.307 (2.24E-15)**	32.970 (3.267E-07)**	136.04 (< 2.2E-16)**
	Peak discharge rate	72.101 (1.514E-15)**	32.419 (4.27E-07)**	137.97 (< 2.2E-16)**
	Lag time	41.263 (5.751E-09)**	5.379 (0.146)	199.52 (< 2.2E-16)**
K_s	Discharge volume	1.231 (0.540)	14.951 (5.668E-04)**	69.388 (8.561E-16)**
	Peak discharge rate	0.178 (0.915)	10.444 (5.395E-03)**	18.104 (1.172E-04)**
	Lag time	0.902 (0.637)	46.442 (8.229E-11)**	0.610 (0.737)
Manning's n	Discharge volume	2.026 (0.363)	0.828 (0.661)	1.878 (0.391)
	Peak discharge rate	0.011 (0.995)	1.101 (0.577)	0.211 (0.900)
	Lag time	1.509 (0.470)	0.327 (0.849)	2.028 (0.363)

Statistical significance of the relationship is noted as: * significant at ≤0.05, and ** at ≤0.01.

Figure 1

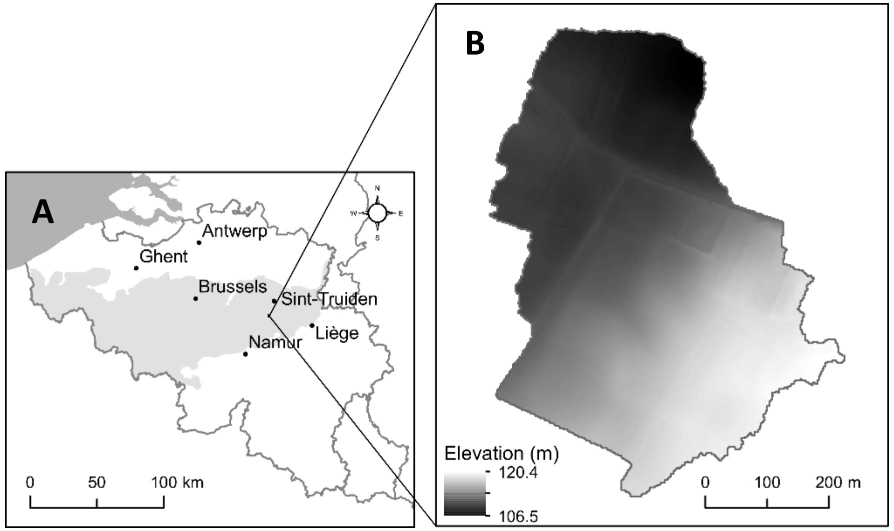
A
Antwerp
Ghent
Brussels
Sint-Truiden
Liège
Namur
0
50
100 km
B
Elevation (m)
120.4
106.5
0
100
200 m

Figure 2

Figure 3

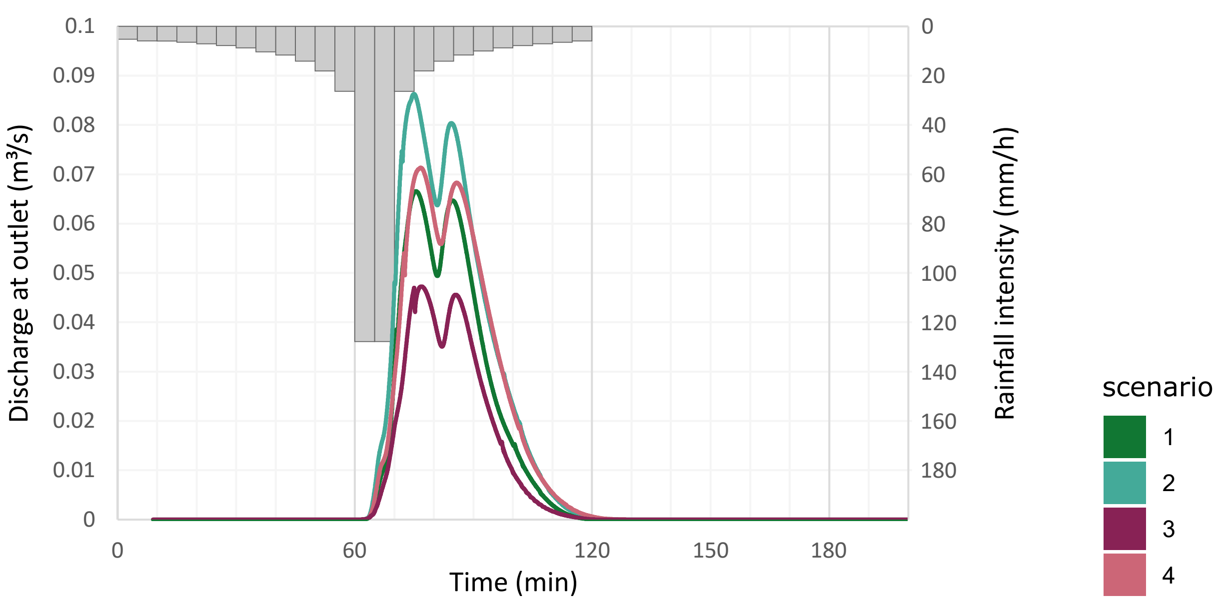

0.1
0.09
0.08
0.07
0.06
0.05
0.04
0.03
0.02
0.01
0
Discharge at outlet (m³/s)
0
20
40
60
80
100
120
140
160
180
Rainfall intensity (mm/h)
0
60
120
150
180
Time (min)
scenario
1
2
3
4

Figure 4

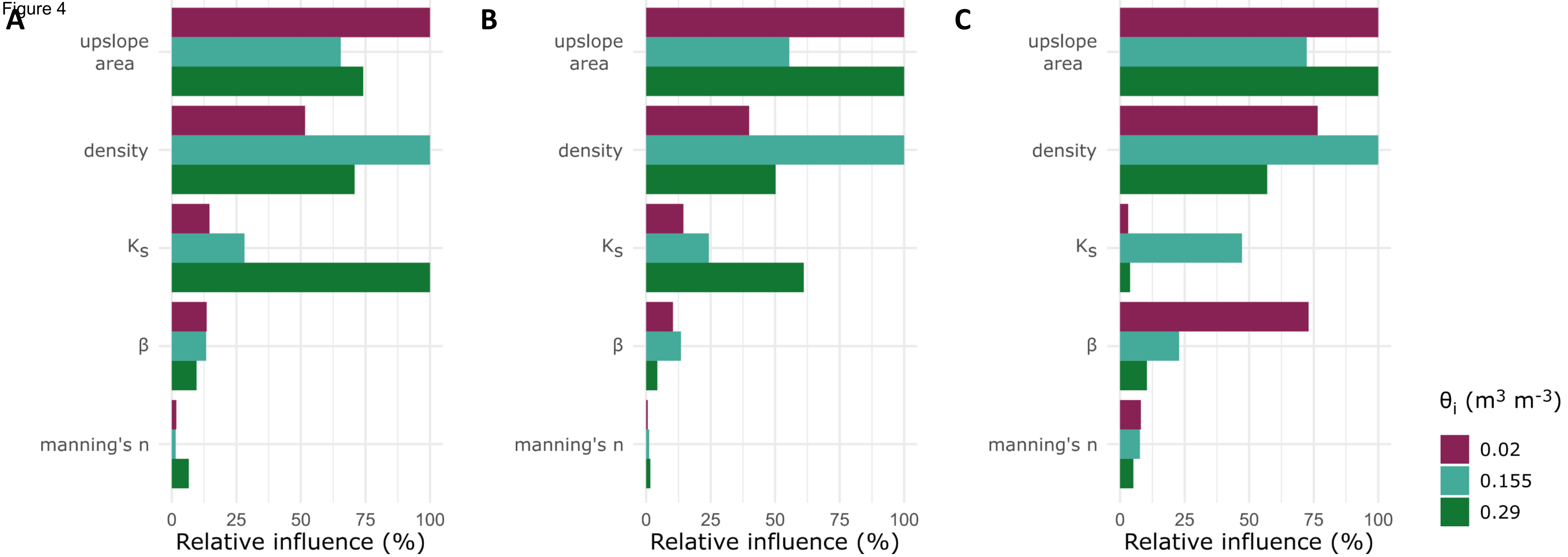
A
B
C
upslope area
density
K_S
β
manning's n
0
25
50
75
100
Relative influence (%)
θ_i (m^3 m^{-3})
0.02
0.155
0.29

Figure 5

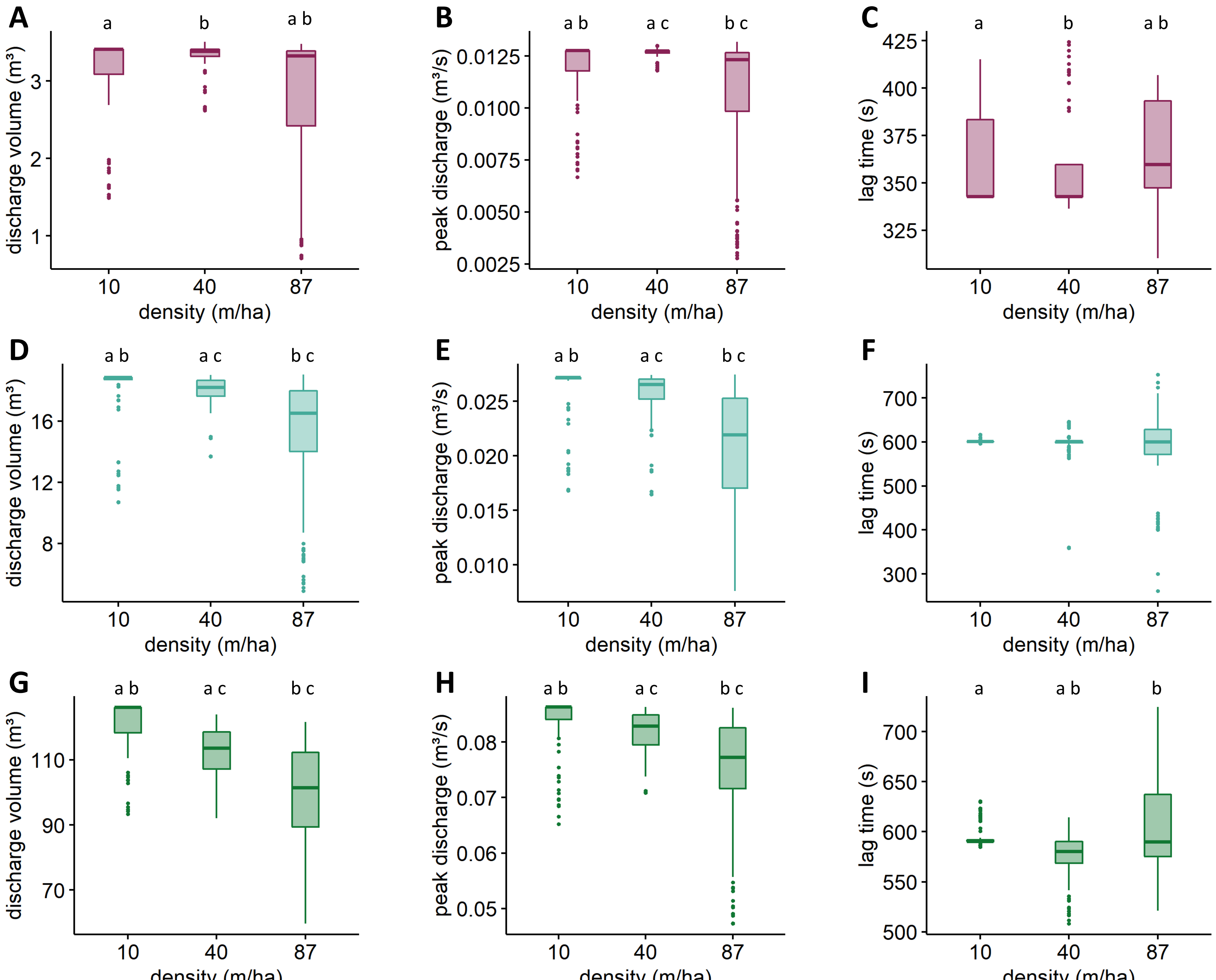
A
a
b
a b
discharge volume (m³)
density (m/ha)
B
a b
a c
b c
peak discharge (m³/s)
density (m/ha)
C
a
b
a b
lag time (s)
density (m/ha)
D
a b
a c
b c
discharge volume (m³)
density (m/ha)
E
a b
a c
b c
peak discharge (m³/s)
density (m/ha)
F
lag time (s)
density (m/ha)
G
a b
a c
b c
discharge volume (m³)
density (m/ha)
H
a b
a c
b c
peak discharge (m³/s)
density (m/ha)
I
a
a b
b
lag time (s)
density (m/ha)

Figure 6

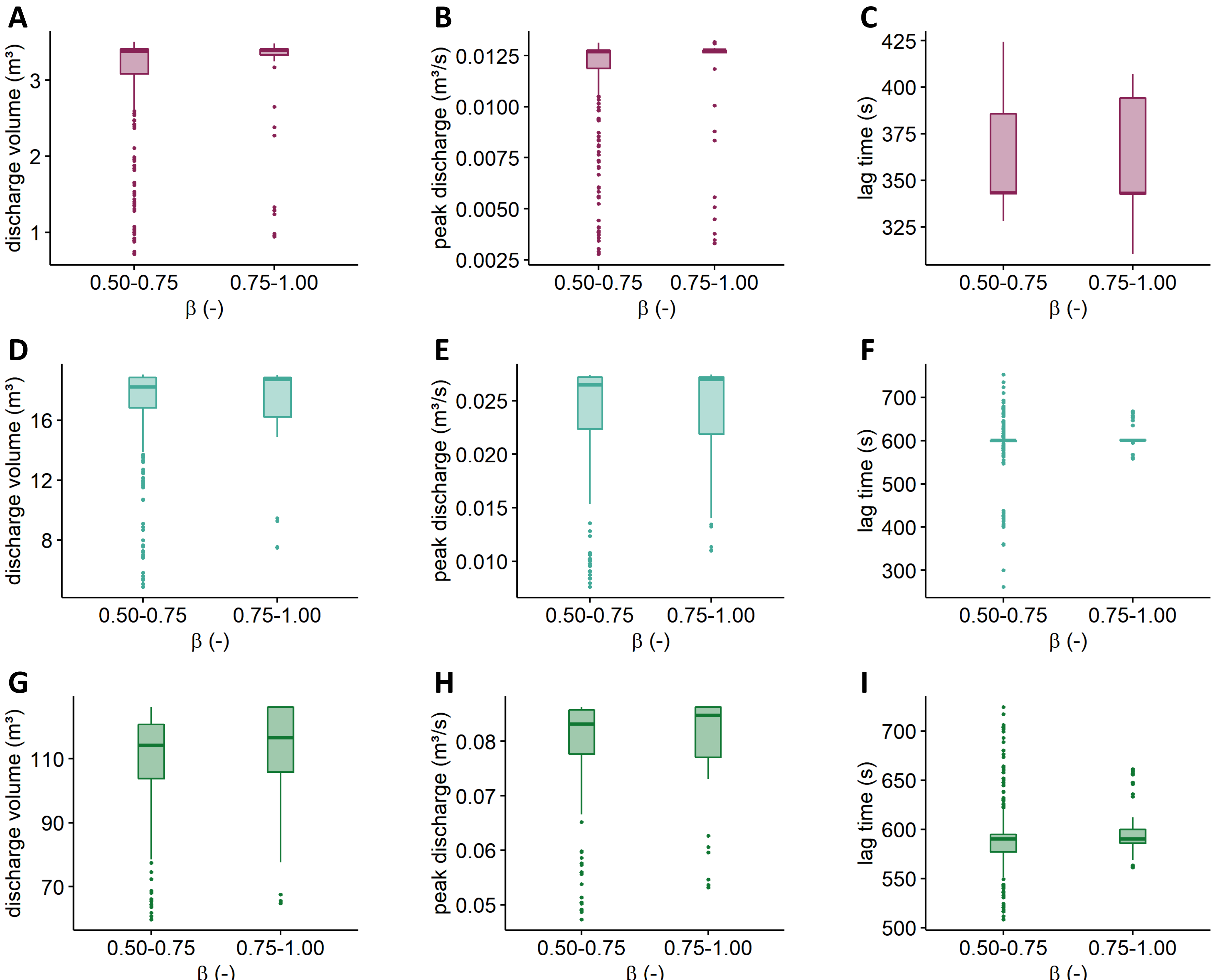

A
discharge volume (m³)
B
peak discharge (m³/s)
C
lag time (s)
D
E
F
G
H
I
0.50-0.75
0.75-1.00
β (-)

Figure 7

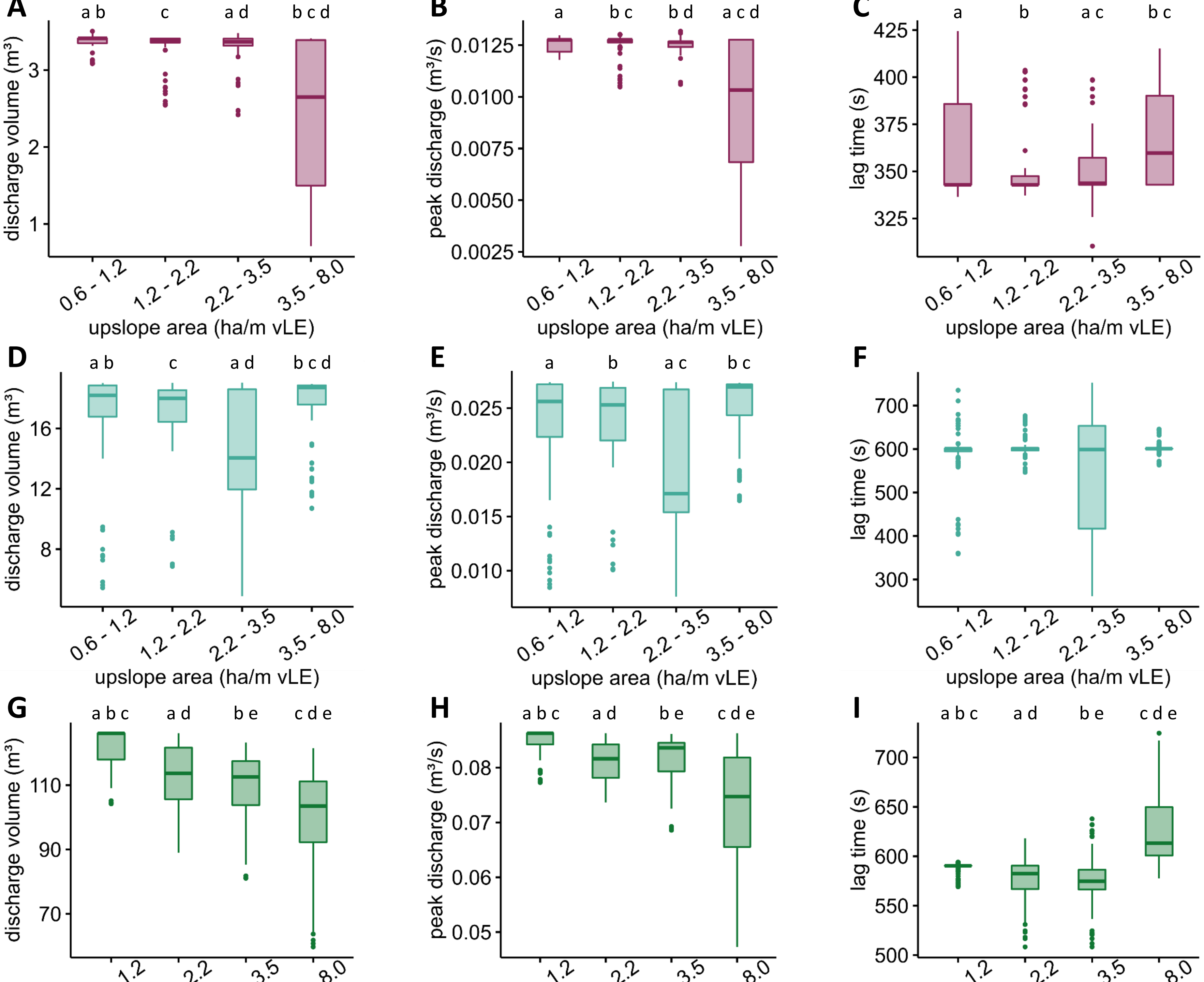
A
B
C
D
E
F
G
H
I
a b
c
a d
b c d
a
b c
b d
a c d
a
b
a c
b c
a b c
a d
b e
c d e
discharge volume (m³)
peak discharge (m³/s)
lag time (s)
upslope area (ha/m vLE)
0.6 - 1.2
1.2 - 2.2
2.2 - 3.5
3.5 - 8.0

Figure 8

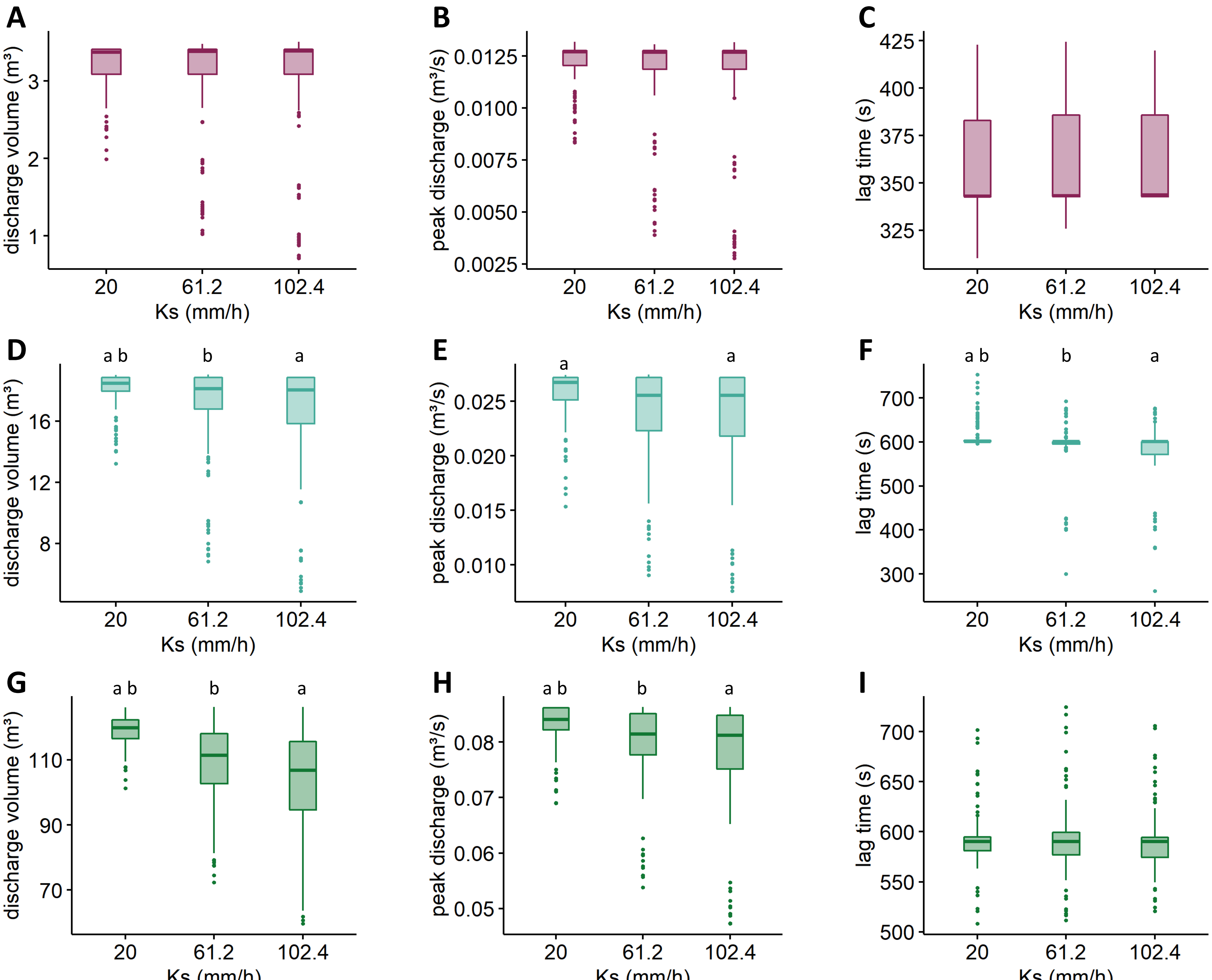

A
B
C
D
E
F
G
H
I
discharge volume (m³)
peak discharge (m³/s)
lag time (s)
Ks (mm/h)
20
61.2
102.4
a b
b
a

Figure 9

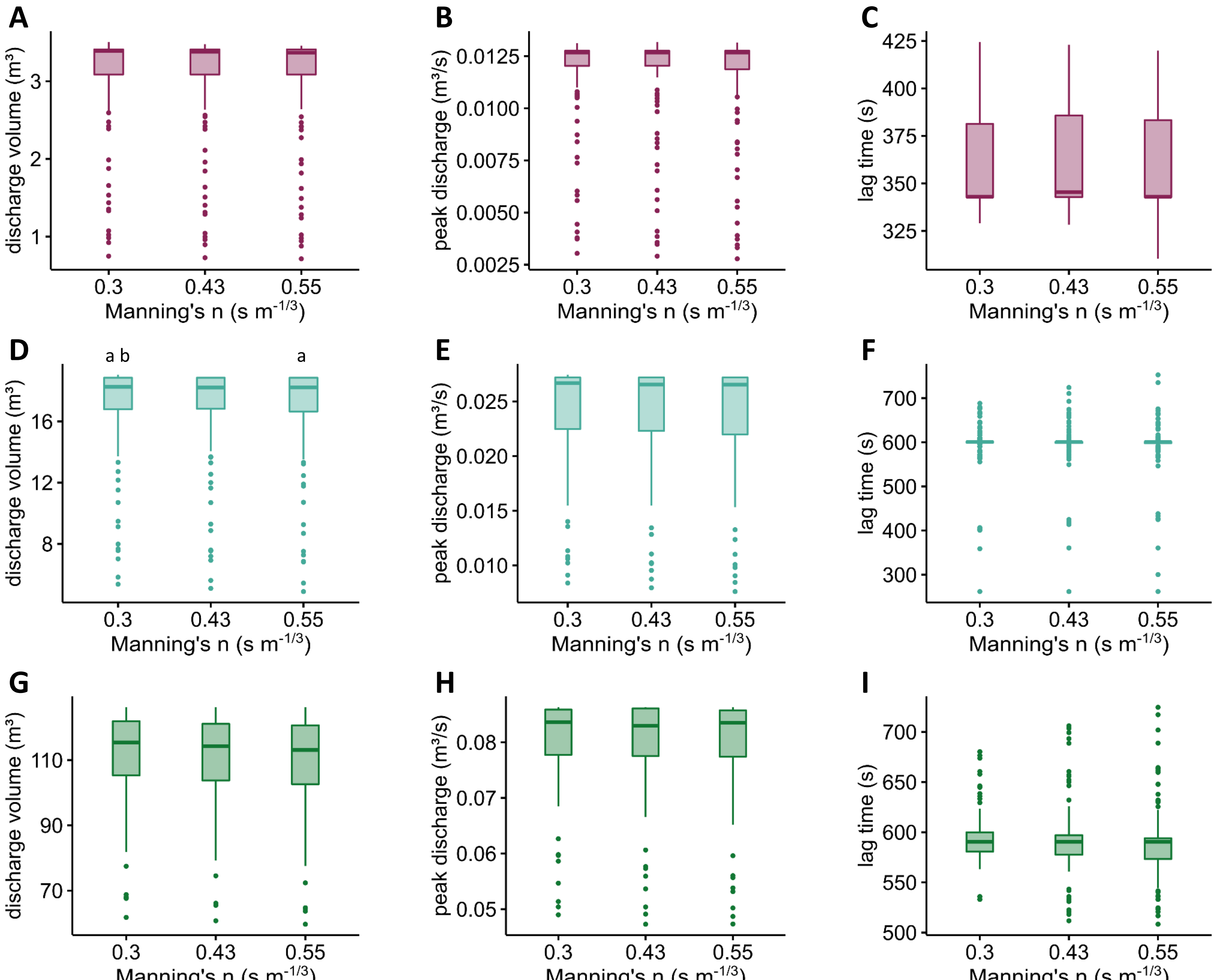

A
B
C
D
E
F
G
H
I
discharge volume (m³)
peak discharge (m³/s)
lag time (s)
Manning's n (s m-1/3)
0.3
0.43
0.55
a b
a

Figure A1

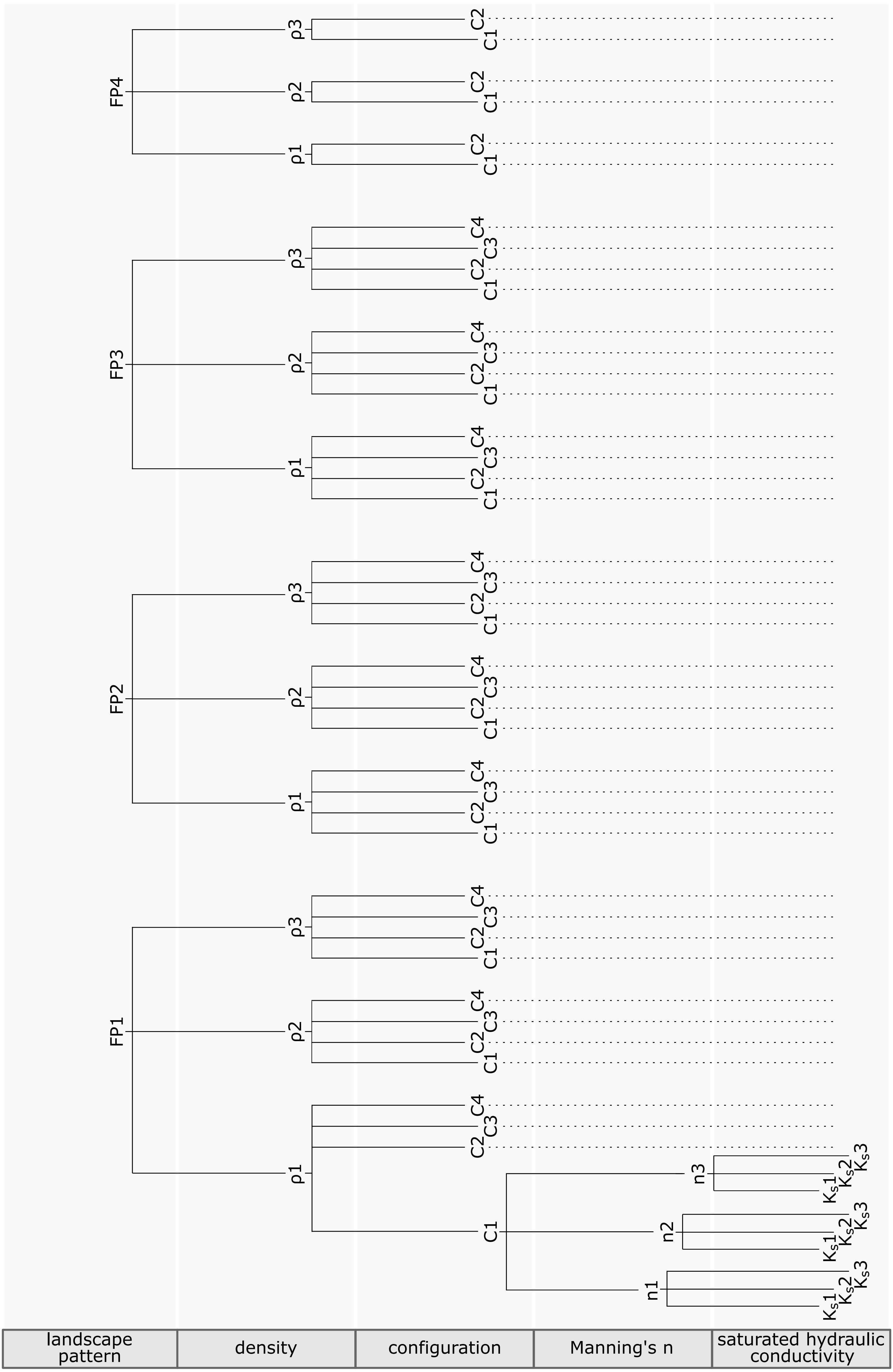

landscape pattern
density
configuration
Manning's n
saturated hydraulic conductivity
FP1
FP2
FP3
FP4
ρ1
ρ2
ρ3
C1
C2
C3
C4
n1
n2
n3
K_s1
K_s2
K_s3

Figure 1. (A) Location of the watershed in the Belgian loess belt (grey) based on Evrard et al. (2007b). (B) Watershed elevation model.

Figure 2. Landscape patterns in (A) FP1, (B) FP2, (C) FP3, and (D) FP4 considered in the watershed.

Figure 3. Discharge at the watershed outlet for four different scenarios detailed in Table 2 and the associated hyetograph for ϑ_i = 0.29 m³ m⁻³.

Figure 4. Global variable importance plots for the prediction of (A) the total discharge volume, (B) the peak discharge rate and (C) the lag time for ϑ_i = 0.02 $m^3 m^{-3}$ (dry soils, purple), ϑ_i = 0.155 $m^3 m^{-3}$ (intermediate wet soils, light green) and ϑ_i = 0.29 $m^3 m^{-3}$ (wet soils, dark green). The five considered variables are 'upslope area': the upslope area of the vLE objects, 'density': the density of the vLE objects in the watershed, 'K_s': the saturated hydraulic conductivity associated with the soil underneath the vLE objects; 'β': the beta-connectivity index of the vLE objects in the watershed, and 'Manning's n': the Manning's roughness coefficient associated with the vLE objects. The different shadings indicate different levels of initial soil moisture content.

Figure 5. Impact of vLE density on total discharge volume, peak discharge rate and lag time for ϑ_i = 0.02 $m^3 m^{-3}$ (A, B & C), ϑ_i = 0.155 $m^3 m^{-3}$ (D, E & F) and ϑ_i = 0.29 $m^3 m^{-3}$ (G, H & I). Lowercase letters above the boxplots show the results of the Dunn's test, with statistically similar (P-value < 0.05) levels grouped by the same letter.

Figure 6. Impact of connectivity expressed as beta connectivity index (β) on total discharge volume, peak discharge rate and lag time for ϑ_i = 0.02 m³ m⁻³ (A, B & C), ϑ_i = 0.155 m³ m⁻³ (D, E & F) and ϑ_i = 0.29 m³ m⁻³ (G, H & I).

Figure 7. Impact of upslope area of the vLEs on total discharge volume, peak discharge rate and lag time for ϑ_i = 0.02 m³ m⁻³ (A, B & C), ϑ_i = 0.155 m³ m⁻³ (D, E & F) and ϑ_i = 0.29 m³ m⁻³ (G, H & I).

Figure 8. Impact of the saturated hydraulic conductivity (K_s) associated with the vLE segments on total discharge volume, peak discharge rate and lag time for ϑ_i = 0.02 m³ m⁻³ (A, B & C), ϑ_i = 0.155 m³ m⁻³ (D, E & F) and ϑ_i = 0.29 m³ m⁻³ (G, H & I). Lowercase letters above the boxplots show the results of the Dunn's test, with statistically similar (P-value < 0.05) levels grouped by the same letter.

Figure 9. Impact of the Manning's roughness coefficient (n) associated with the vLE segments on total discharge volume, peak discharge rate and lag time for ϑ_i = 0.02 m³ m⁻³ (A, B & C), ϑ_i = 0.155 m³ m⁻³ (D, E & F) and ϑ_i = 0.29 m³ m⁻³ (G, H & I).

Figure A.1 Overview of the 378 scenarios used in this study.